International Journal of Rock Mechanics and Mining Sciences 119 (2019) 205–210

Contents lists available at ScienceDirect

International Journal of Rock Mechanics and Mining Sciences

journal homepage: www.elsevier.com/locate/ijrmms

# Relationships between mechanical and transport properties in Marcellus shale

B. Schwartz*, D. Elsworth, C. Marone

*G3 Center, The Pennsylvania State University, University Park, USA*

ABSTRACT

We explore relationships among bulk modulus, crack density, and permeability through repetitive loading of Marcellus shale. Cumulative cyclic stressing (22–26 MPa with confinement of 24 MPa) is applied at a frequency of 0.05 Hz over 100,000 cycles. Changes in acoustic velocities are used to follow changes in dynamic bulk modulus, Poisson ratio, and crack density and to correlate these with bedding-parallel measurements of methane permeability. The shale is represented as an orthotropic elastic medium containing a dominant, noninteracting fracture set separated by thin laminae. An effective continuum model links permeability evolution to the evolution of the bulk modulus and crack density. Bulk modulus is linearly related to crack density by a scaling parameter representing rock fabric and fracture geometry. The Poisson ratio and bulk modulus of the intact, uncracked shale are approximated from our data. We propose a method for tracking permeability evolution of finely laminated shales using acoustic waves.

## 1. Introduction

Laminated shale can be characterized as an orthotropic material with a dominant fracture set oriented parallel to bedding.[1,2] While not all shales can be characterized by this model, it has successfully been applied to Marcellus, Tournemire, and Bakken shale.[1,3,4] The orthotropy results from nanometer to micrometer-wide bedding-parallel fractures separated by finely laminated thin stacks of minerals.[5,6] Ultrasonic measurements confirm this orthotropy, often manifest as anisotropy based on the contrast between bedding-parallel laminations[4] and properties perpendicular to bedding.[7]

The presence of fractures has been shown to influence both the mechanical and transport properties of rocks, to increase the anisotropy, with correlations apparent between elastic wave velocities and permeability.[8] Permeability and compressional velocity both increase as the angle to bedding increases from perpendicular to parallel.[9] The permeability of shale has been shown to be up to 10–100 times higher parallel to bedding than perpendicular to bedding.[10–12] Shales are also observed to be approximately twice as stiff parallel to bedding than perpendicular to it.[13] Codifying such correlations between permeability and stiffness in Marcellus shale, via wave-speed measurements, is the focus of this work.

We use the influence of crack density on material properties[14,15] to link stiffness and permeability. Crack density may be considered a scalar, a vector, a second rank tensor, or a fourth rank tensor depending on the application.[16,17] For the special case of a cracked material[18] with non-interacting, parallel fracture sets[16,19] the elastic response is orthotropic or anisotropic and characteristic of shales.[20]

Various models relate crack density to permeability[21] and to material stiffness[22,23] with crack densities and permeability measured simultaneously.[24] For changes in state, the evolution of seismic velocities and permeability have both been used to measure crack density evolution, dilatancy, and crack propagation in granites, rock salt, and basalt.[25–27] Here, we explore the relationships among permeability, bulk modulus, and crack density in order to develop a method to track permeability evolution based on changes in geometry of the fracture network that impact the mechanical state of the solid.

## 2. Methods

We used cylindrical samples of Marcellus shale (19 mm in diameter and 16 mm in length, cut with bedding parallel to the cylinder axis) and subjected them to triaxial loading in a standard pressure vessel as shown in Fig. 1 with custom components for simultaneous measurement of permeability and elastic wave properties. Native water saturation was less than 3% and considered negligible. The sample was loaded hydrostatically to 24 MPa and allowed to compact for a week in order to eliminate creep from measurements. Using methane as the saturating fluid, a suite of permeability measurements was conducted throughout the experiment at a constant pore pressure of 6 MPa using the pressure pulse method[28]:

$$k = \frac{\mu\beta\alpha L}{A}\frac{V_{up}V_{dn}}{V_{up}+V_{dn}}. \quad (1)$$

* Corresponding author.110 Hosler Building, University Park 16802.
*E-mail address:* schwartz@psu.edu (B. Schwartz).

https://doi.org/10.1016/j.ijrmms.2019.04.020
Received 5 December 2018; Received in revised form 28 February 2019; Accepted 29 April 2019

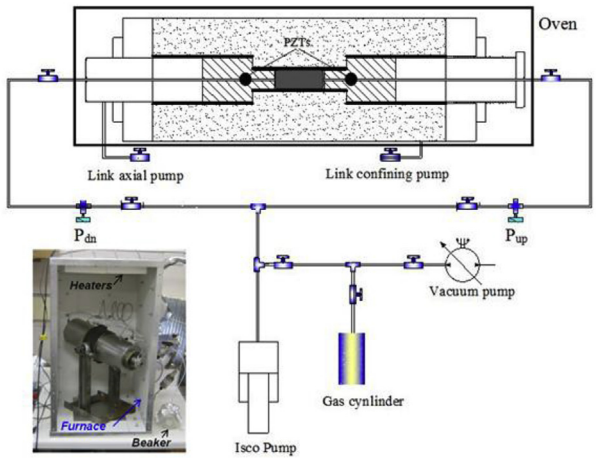


**Fig. 1.** Experimental setup. A cylindrical sample of Marcellus shale measuring 19 mm in diameter and 16 mm in length was loaded into a triaxial stress vessel. The vessel was housed in a temperature-controlled oven to keep temperature constant at 21 °C. PZT's were installed in the end platens in order to measure acoustic velocities concurrently with permeability measurements. Stress was automatically cycled in 10 s bursts along the longitudinal axis of the sample ± 2 MPa over the 24 MPa confining stress. Pore pressure was kept constant at 6 MPa with methane as the saturating fluid.

where $k$ is permeability in $m^2$, $\mu$ is gas viscosity in Pa·s, $\beta$ is gas compressibility in $Pa^{-1}$, $\alpha$ is the slope of the pressure pulse decay in $s^{-1}$, $L$ is the sample length in meters, $A$ is the sample's cross-sectional area in $m^2$, and $V_{up}$ and $V_{dn}$ are the upstream and downstream reservoir volumes, respectively, measured in $m^3$. The upstream and downstream volumes were determined using the real gas law. Values for $\mu$ and $\beta$ were determined with NIST's online thermophysical properties software for pore pressure of 6 MPa and room temperature of 21 °C. During the permeability measurements, upstream and downstream pressures were set to 6.3 MPa and 5.7 MPa respectively. Permeability measurements required approximately 1 h each, after which time the experiment was set up to automatically begin cycling the axial stress again. Pore pressure was kept constant at 6 MPa during the stress cycling portions of the experiment.

Permeability measurements were made concurrently with measurements of elastic properties. We used 500 kHz central frequency piezoelectric transducers to measure acoustic travel times, bulk modulus $K$, and Poisson ratio, $\nu$, where:

$$\bar{K} = \rho\left(V_p^2 - \frac{4}{3}V_s^2\right). \tag{2}$$

and

$$\bar{\nu} = \frac{V_p^2 - 2V_s^2}{2(V_p^2 - V_s^2)}. \tag{3}$$

In a continuum framework containing cracks, $\bar{K}$ is the cracked bulk modulus, $\bar{\nu}$ is the cracked Poisson ratio, and ρ is the shale density, which we measured to be 2600 $kg/m^3$. $V_p$ and $V_s$ are the compressional wave velocity and shear wave velocity, respectively. The cracked Poisson ratio was used to calculate the crack density parameter at each time step. We used the scalar definition of the crack density parameter $\varepsilon$ for long narrow elliptic cracks[17,18]:

$$\varepsilon = \frac{45}{8}\frac{\nu - \bar{\nu}}{(1 - \bar{\nu})(10\nu - 8\nu\bar{\nu} - \bar{\nu})}. \tag{4}$$

where $\bar{\nu}$ is the measured Poisson ratio of the cracked medium and $\nu$ is the corresponding Poisson ratio of the intact rock, which in this case was approximated to be 0.284. In the cracked continuum literature, "intact" refers to a rock with zero porosity. Materials behave differently in the absence of cracks, and no rock is truly intact in that sense. However, we show below that a valid approximation for the intact Poisson ratio can be made.

After samples compacted under hydrostatic load, we made initial measurements of permeability, bulk modulus, and Poisson ratio. At constant pore pressure, we then began to cycle the external axial stress longitudinal to the core's length from 22 to 26 MPa in 10 s bursts while keeping the confining stress around the circumference of the core at 24 MPa. This process was automated, such that we were able to cycle the stress approximately 4000 times a day. There was a period of quiescence from days 10–20, to allow further monitoring of compaction during hydrostatic stressing. In 37 days, approximately 100,000 cycles were performed on the sample. Measurements for material properties were conducted once per day. Once Poisson ratio measurements were cross-plotted with permeability measurements, we were able to approximate the "intact" Poisson ratio to solve Eq. (4).

## 3. Results

Our basic data set consists of deformation measurements and the evolution of material properties as a function of time during hydrostatic loading with small amplitude stress cycles. We focus on the relationship between bulk modulus, permeability, and crack density and show that bulk modulus and crack density follow a linear relationship. Two of the unknowns—intact bulk modulus and intact Poisson ratio—can be approximated from our data.

### 3.1. Evolution of material properties over time

In order to calculate the intact Poisson ratio, the measured Poisson ratio was cross-plotted with permeability as shown in Fig. 2. The intact Poisson ratio is an idealization of the cracked continuum literature representing the Poisson ratio of a rock with zero porosity. Points in Fig. 2 can be selected as permeability approaches $10^{-22}$ $m^2$, which is considered a lower limit on measurable permeability—at values less than $10^{-22}$ $m^2$, pore spaces are so small that they begin to approach the "intact" idealization from the cracked continuum literature. In Fig. 2 we show that on an extrapolated line from the measured data, this sample's intact Poisson ratio can be approximated to be between 0.273 and 0.294. We select the mid-point of 0.284 as an approximation of the intact Poisson ratio in order to calculate the crack density parameter.

Fig. 3 shows the evolution of material properties over time—permeability is plotted on the right axis on a logarithmic scale. The permeability dropped from an initial value of $6.7 \times 10^{-18}$ $m^2$ to a final value of $3.0 \times 10^{-20}$ $m^2$: a 233-fold decrease. The shape of the permeability curve shows faster permeability reduction at early times—one order of magnitude in the first few days. The crack density is also plotted in Fig. 3 and over the experiment ranges from a starting value of 0.185 to 0.102—a 45% reduction. The permeability and crack density scale directly with each other, as do the bulk modulus and Poisson ratio. The bulk modulus ranged from a starting value of 12.1 GPa–15.1 GPa and the Poisson ratio ranged from 0.197 to 0.237.

### 3.2. Evolution of permeability plotted against changing material properties

We monitored the evolution of permeability and acoustic travel time throughout the experiment. Each measurement is taken at the same effective stress, as the sample is returned to its original state of stress of 24 MPa hydrostatic external stress and 6 MPa pore pressure before measurements are taken. Differences in transport and mechanical properties should be understood to result from plastic deformation occurring during the cyclic compression. Fig. 4 shows the evolution of permeability as a function of evolving material properties and acoustic travel times. Fig. 4a shows the permeability evolution as a function of crack density. Permeability evolution is plotted on a logarithmic scale, and the figure shows that as crack density decreases linearly, permeability decreases logarithmically. Permeability is decreasing because

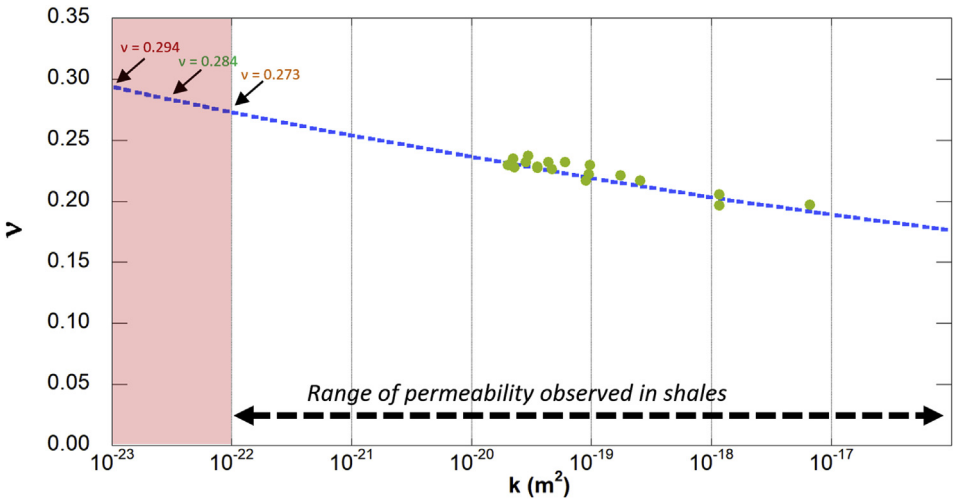


**Fig. 2.** As a rock's permeability approaches $10^{-22}\,m^2$, pores become so small that they can be treated as "intact" or "pristine." In the cracked continuum literature, "intact" refers to an idealized rock that has zero porosity. Here we cross plot measured values of permeability with Poisson ratio and extrapolate to the impermeable transition where shale can be idealized as pristine. We select three Poisson ratio values with permeability between $10^{-23}\,m^2$ and $10^{-22}\,m^2$ and use the midpoint value of $\nu$ equal to 0.284 as the intact Poisson ratio to continue the analysis.

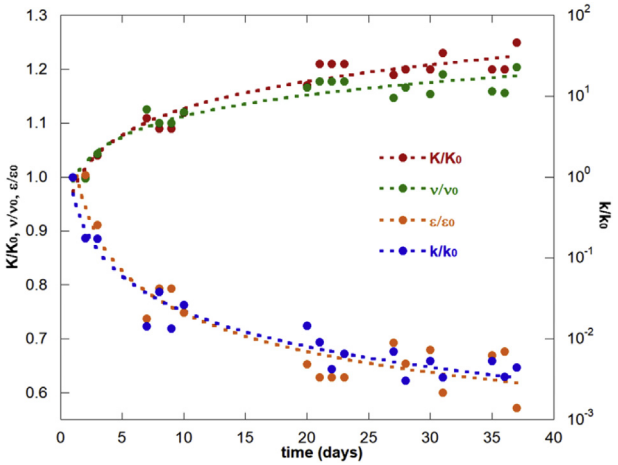


**Fig. 3.** Evolution of material properties over time. Bulk modulus and Poisson ratio follow similar trends. The crack density is plotted on Cartesian axes while the permeability is plotted on semi-log axes: crack density evolution scales with the permeability evolution.

pore spaces are becoming smaller, which also results in a lower crack density parameter. Similarly, as bulk modulus increases linearly in Fig. 4b, permeability decreases linearly. This is consistent with shortening of the semi-major axis length of a non-circular pore—as the length decreases, the rock becomes stiffer. Acoustic wave speeds are plotted against permeability evolution in Fig. 4c and d. We note that as the P-wave velocity increased from 3.0 to 3.3 km/s, the permeability decreased two and a half orders of magnitude. As this sample is loaded parallel to bedding, we see a much larger change in $V_p$ (Fig. 4c) over the experiment than we do in $V_s$ (Fig. 4d). These plots are consistent with fracture closure and fracture shortening—reduction in both the semi-major and semi-minor axis lengths of ellipsoid pores. This is clearly seen in Fig. 4b comparing bulk modulus to permeability evolution: fractures close (decreased aperture $b$) as permeability evolution decreases and fracture length $a$ shortens as bulk modulus increases.

### 3.3. Relationship between bulk modulus, crack density, and intact Poisson ratio

In Fig. 5 we find that for our experiment bulk modulus varies linearly with crack density and can be cast in the following slope-intercept form:

$$\bar{K} = K(1 - \alpha\varepsilon). \tag{5}$$

where $\bar{K}$ is the measured bulk modulus of the cracked medium, $K$ is the intact bulk modulus, $\varepsilon$ is the dimensionless crack density parameter, and $\alpha$ is a constant—in this case equal to 2.0. In the classic slope-intercept form, the slope m is $-K\alpha$ in Eq. (5). Since both $K$ and $\alpha$ are constants, their product is also a constant. It is expected that different rocks will have values of $K\alpha$, which will be seen when cross plotting measured bulk modulus with crack density. This suggests that $\alpha$ is related to material properties including rock fabric and bedding orientation, and that the parameter α depends on the matrix and fluid properties, the geometry of the cracks, and the interactions between them.[29,30] Also plotted in Fig. 5 is bulk modulus vs. cracked Poisson ratio. The value of the bulk modulus at the intact Poisson ratio of 0.284 is 19.0 GPa and corresponds to the value of the "intact" bulk modulus in the absence of cracks.

## 4. Discussion

Here we explore the relationships among three measured rock properties and the subsequent evolution of mechanical and transport properties after applying a cyclic deviatoric stress to a sample of Marcellus shale. Our findings indicate that the relationship between bulk modulus and crack density in our experiment is linear. We apply an effective continuum model to relate the bulk modulus and the permeability through the crack density parameter. We use the scalar definition of crack density set out by O'Connell and Budiansky[17] due to its popularity, ease of implementation, and applicability to orthotropic materials with noninteractive fractures. In order to relate crack density to permeability, we cast crack density in terms of the area and perimeter of an ellipsoidal crack. The aperture of the ellipse is then defined in terms of the crack density. We find that for our experiment, permeability evolution can be related to crack density evolution.

### 4.1. Finding the unknowns K and ν

In Eqs. (1)–(5) there are three unknowns: intact bulk modulus $K$, intact Poisson ratio $\nu$, and the slope $\alpha$ of the $K$ vs. $\varepsilon$ curve in Fig. 5. We approximate the intact Poisson ratio to be 0.284 from Fig. 2. The intact Poisson ratio corresponds to the value of the measured Poisson ratio when crack density is zero (Fig. 5). Plotting bulk modulus vs. measured Poisson ratio, the intact bulk modulus is that value of $K$ that corresponds to the intact Poisson ratio at a crack density of zero. Therefore, the intact bulk modulus is equal to 19.0 GPa. The value of the slope α can be found directly by solving Eq. (5). In this case, α is 2.0. This is a useful scheme because the system unknowns are reduced to measured values.

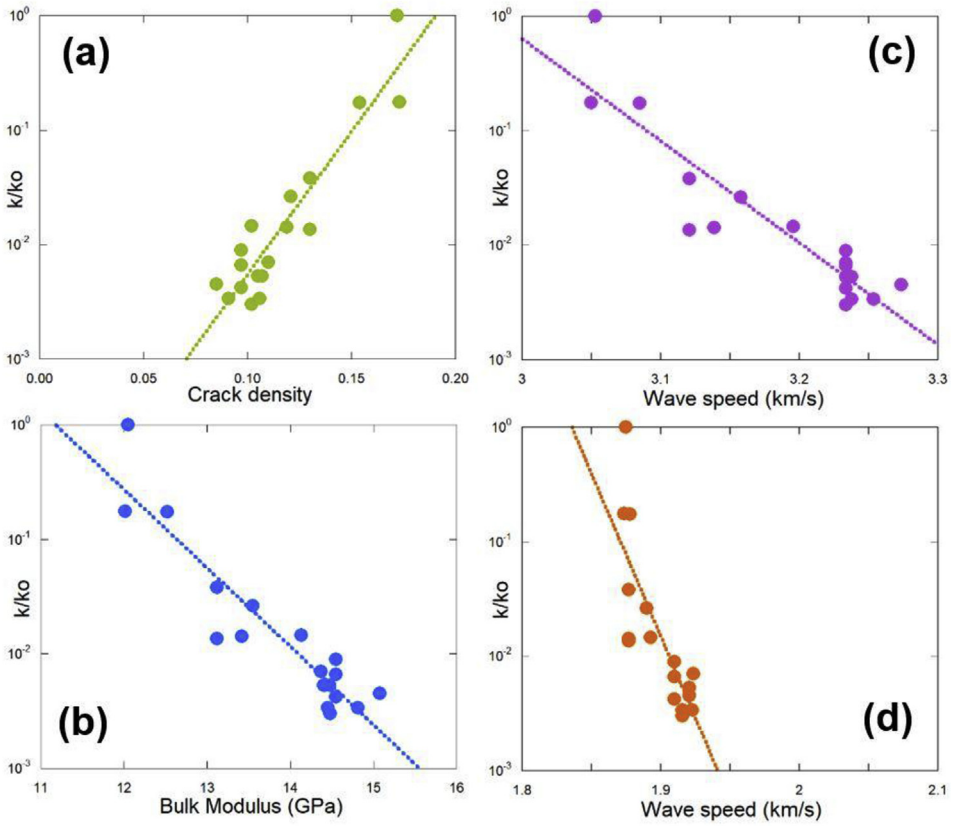


**Fig. 4.** Mechanical properties plotted against permeability evolution. (a) Top-left, shows permeability reduction as crack density decreases, largely driven by changes in fracture aperture. (b) Bottom-left, shows bulk modulus increasing as permeability decreases, indicating that mechanical stress cycling led to a reduction in both the fracture length and fracture aperture. (c) and (d), top-right and bottom-right, respectively, show the change in acoustic wave speeds as permeability was reduced.

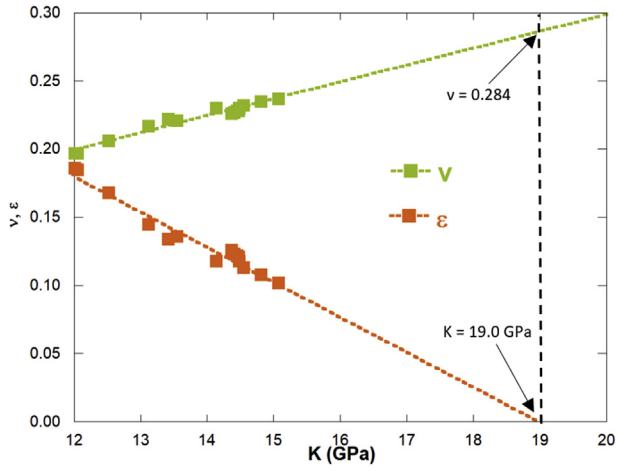


**Fig. 5.** Bulk modulus vs. crack density and Poisson ratio. The data indicate linear relationships and show the values of the intact bulk modulus and intact Poisson ratio. Interchanging the axes would show that the bulk modulus and crack density parameter are related through Eq. (5).

### 4.2. Relating crack density to permeability

The definition of the crack density parameter suggests that permeability must change with a change in crack density. While Eq. (4) has limitations—cracks are assumed parallel and the medium must be orthotropic—these limitations vanish as a rock approaches the idealizations of these two assumptions.[16,31] Both the Poisson ratio and the bulk modulus can be measured with acoustic waves. In order to relate the crack density to the permeability, we recast the crack density parameter using the geometric interpretation below. In O'Connell and Budiansky[17] crack density is defined as:

$$\varepsilon = \left(\frac{2N}{\pi}\right)\left(\frac{A^2}{P_{el}}\right) \tag{6}$$

where $N$ is the number of cracks per unit volume, $A$ is the area of an ellipsoid crack $\pi ab$, and $P_{el}$ is the perimeter of the ellipsoid. Rearranging for $b$:

$$b^2 = \frac{\varepsilon P_{el}}{2N\pi a^2} \tag{7}$$

If a circle with radius b and perimeter 2πb is inscribed into the ellipsoid, with $P_{el} > P_c$, then

$$b > \frac{\varepsilon}{Na^2} \tag{8}$$

In the absence of the generation of new cracks, $N$ is a constant such that dividing $b$ by $b_0$ gives

$$\frac{b}{b_0} = f\left(\frac{\varepsilon}{\varepsilon_0}\right)\frac{\varepsilon}{\varepsilon_0}\frac{a_0^2}{a^2} \tag{9}$$

where $f$ is a function to track crack density evolution and, thereby, remove the inequality sign. In the case of penny shaped cracks

$$\frac{a_0}{a} = \frac{E}{E_0} = \frac{(1-2\nu)}{(1-2\nu_0)}\frac{K}{K_0} \tag{10}$$

Casting flow in the bedding parallel direction as Darcian flow between parallel plates, the cubic law holds such that

$$\frac{k}{k_0} = \left(\frac{b}{b_0}\right)^3 \tag{11}$$

and we can cast permeability evolution in terms of the crack density evolution:

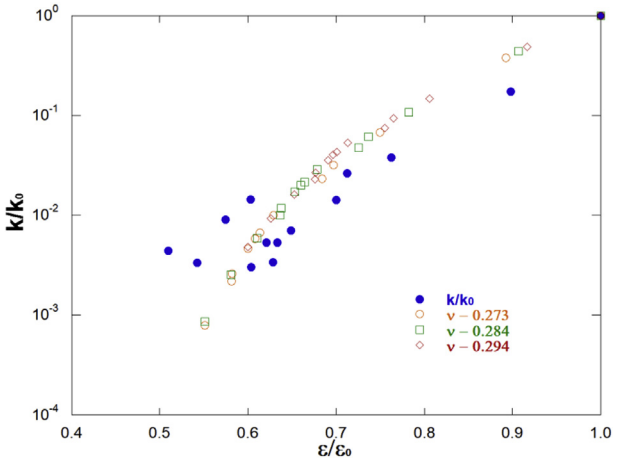


**Fig. 6.** Measured and predicted permeability evolution plotted against crack density evolution $\varepsilon/\varepsilon_0$. The predicted permeability in Eq. (12) is independent of our choice of intact Poisson ratio as seen by all values for $\nu$ collapsing to a single curve. This allows the $\beta$ in Eq. (13) to be deduced based on its fit to the experimental data.

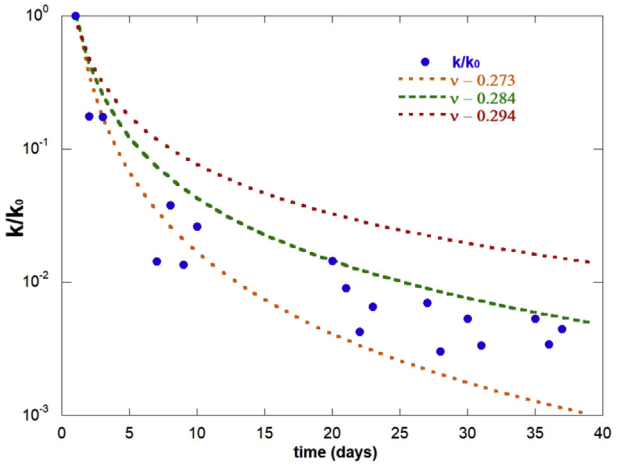


**Fig. 7.** Permeability evolution vs. time for three different values of intact Poisson ratio, where the projected curves are values from Eq. (12) that differ as the pick for intact Poisson ratio changes the value of the crack density parameter from Eq. (4). We see that the experimental data suggest that the value for the intact Poisson ratio falls between 0.273 and 0.284.

$$\frac{k}{k_0} = \left( f\left(\frac{\varepsilon}{\varepsilon_0}\right) \frac{\varepsilon}{\varepsilon_0} \frac{(1-2\nu)^2}{(1-2\nu_0)^2} \frac{K^2}{K_0^2} \right)^3 = \left( f\left(\frac{\varepsilon}{\varepsilon_0}\right) \frac{\varepsilon}{\varepsilon_0} \frac{(1-2\nu)^2}{(1-2\nu_0)^2} \frac{(1-\alpha\varepsilon)^2}{(1-\alpha\varepsilon_0)^2} \right)^3 \tag{12}$$

The crack density evolution function $f(\varepsilon/\varepsilon_0)$ captures te departure of the fracture set from the idealized geometries used to form the above equations. A realistic constraint on this linear function would be that $f(\varepsilon_0/\varepsilon_0) = 1$, suggesting an equation of the form

$$f\left(\frac{\varepsilon}{\varepsilon_0}\right) = (1+\beta)\frac{\varepsilon}{\varepsilon_0} - \beta \tag{13}$$

where $\beta$ is a constant between 0 and 1; $\beta$ is a property of the rock fabric, geometry, and the tortuosity of the flow channels. A large $\beta$ value corresponds to a system where the change in aperture is much larger than that suggested by the idealized case.

We plot Eq. (12) for the three values of intact Poisson ratio picked in Fig. 2. We note in Fig. 6 that all three curves collapse to a single curve when plotting versus crack density evolution, allowing us to optimize the value of $\beta$ independent of our choice of intact Poisson ratio. For this experiment, a $\beta$ of 0.75 captures the permeability evolution in Eq. (12) with an excellent fit, as seen in Fig. 6. In Fig. 7, permeability evolution is plotted versus time. The original data from the experiment is marked by blue circles and the projected permeability evolution from Eq. (12) is shown for our three original picks for intact Poisson ratio. While all values of assumed intact Poisson ratio collapsed to a single curve in Fig. 6, each value projects a different curve in Fig. 7 and shows that the actual value of the intact Poisson ratio is between 0.273 and 0.284.

## 5. Conclusion

We mechanically stressed Marcellus shale to explore the evolution of transport and mechanical properties over time. We also explored the evolution of transport properties in Marcellus shale as a function of the evolution of these mechanical properties. Our findings show relationships among bulk modulus, permeability, and crack density. We derived a model to relate permeability evolution to the product of stiffness evolution and crack density evolution using geometric arguments. In summary: Crack density scales directly with permeability. Crack density has a linear relationship with bulk modulus. The scaling parameter $\alpha$ is related to rock properties. Both the intact bulk modulus and intact Poisson ratio can be approximated from cross plots. Permeability is cast in terms of mechanical property evolution cubed.

Marcellus shale offers a unique opportunity for characterization because of its severe orthotropy and dominant fracture set oriented parallel to bedding. Measuring permeability in this orientation provides a useful analog to hydrocarbon production in a reservoir in which the shale is also oriented with flow occurring parallel to bedding. The use of the crack density parameter also offers insights into hydrocarbon movement from the matrix into hydraulic fractures. The Marcellus shale studied here represents an orthotropic material with a dominant fracture set in the bedding parallel direction. The orientation of the dominant fracture set will have a significant impact on the evolution of permeability and mechanical properties. While these experimental results are not enough to reach a representative conclusion of all rock behavior, we suggest that more work be done to expand the range over which permeability can be tracked with acoustic velocities.

The relationships explored here are relevant to exploration geologists, geophysicists, seismologists and others. We have related permeability evolution solely to acoustic velocities and deduced constants: $\alpha$, $K$, and $\nu$. Perhaps the most immediate opportunity to apply this research is in reservoir characterization, where well logs and fiber optics cables both measure acoustic velocities. The work presented here suggests that these velocities can be used to monitor permeability evolution indirectly and provides a second method to calculate permeability evolution in conjunction with pressure and production data.

## Acknowledgements

This work is the result of support from the Chevron Energy Technology Company. This support is gratefully acknowledged.

## References

1. Bonnelye A, Schubnel A, David C, Henry P, Guglielmi Y, et al. Elastic wave velocity evolution of shales deformed under uppermost crustal conditions. *J Geophys Res: Solid Earth.* 2017;122(1):130–141.
2. Crook AJ, Yu JG, Willson SM. Development of an orthotropic 3D elastoplastic material model for shale. *SPE/ISRM Rock Mechanics Conference.* Society of Petroleum Engineers; 2002.
3. Kuma H, Elsworth D, Mathews JP, Marone C. Permeability evolution in sorbing media: analogies between organic-rich shale and coal. *Geofluids.* 2016;16(1):43–55.
4. Bandyopadhyay K. *Seismic Anisotropy: Geological Causes and its Implications to Reservoir Geophysics* PhD thesis Stanford University; 2009.
5. Horne SA. A statistical review of mudrock elastic anisotropy. *Geophys Prospect.* 2013;61(4):817–826.
6. Ulm FJ, Abousleiman Y. The nanogranular nature of shale. *Acta Geotechnica.* 2006;1(2):77–88.
7. Vanorio T, Mukerji T, Mavko G. Emerging methodologies to characterize the rock physics properties of organic-rich shales. *Lead Edge.* 2008;27(6):780–787.

8. Gueguen Y, Schubnel A. Elastic wave velocities and permeability of cracked rocks. *Tectonophysics.* 2003;370(1-4):163–176.
9. Tutuncu AN, Mese AI. Relationship between permeability, acoustic, mechanical and strength anisotropies in unconventional reservoirs and seal shales. *45th US Rock Mechanics/Geomechanics Symposium.* American Rock Mechanics Association; 2011.
10. Bolton AJ, Maltman AJ, Fisher Q. Anisotropic permeability and bimodal pore-size distributions of fine-grained marine sediments. *Mar Petrol Geol.* 2000;17(6):657–672.
11. Kwon O, Kronenberg AK, Gangi AF, Johnson B, Herbert BE. Permeability of illite--bearing shale: 1. Anisotropy and effects of clay content and loading. *J Geophys Res: Solid Earth.* 2004;109(B10).
12. Pan Z, Ma Y, Connell LD, Down DI, Camilleri M. Measuring anisotropic permeability using a cubic shale sample in a triaxial cell. *J Nat Gas Sci Eng.* 2015;26:336–344.
13. Sone H, Zoback MD. Mechanical properties of shale-gas reservoir rocks—Part 1: static and dynamic elastic properties and anisotropy. *Geophysics.* 2013;78(5):D381–D392.
14. Bristow JR. Microcracks, and the static and dynamic elastic constants of annealed and heavily cold-worked metals. Br J Appl Phys; 11(2): 81.
15. Walsh JB. The effect of cracks on the compressibility of rock. *J Geophys Res.* 1965;70(2):381–389.
16. Kachanov M. Effective elastic properties of cracked solids: critical review of some basic concepts. *Appl Mech Rev.* 1992;45(8):304–335.
17. O'Connell RJ, Budiansky B. Seismic velocities in dry and saturated cracked solids. *J Geophys Res.* 1974;79(35):5412–5426.
18. Budiansky B, O'Connell RJ. Elastic moduli of a cracked solid. *Int J Solids Struct.* 1976;12(2):81–97.
19. Piau M. Crack-induced anisotropy and scattering in stressed rocks: effective elastic moduli and attenuation. *Int J Eng Sci.* 1980;18(4):549–568.
20. Hornby BE, Schwartz LM, Hudson JA. Anisotropic effective-medium modeling of the elastic properties of shales. *Geophysics.* 1994;59(10):1570–1583.
21. Gueguen Y, Dienes J. Transport properties of rocks from statistics and percolation. *Math Geol.* 1989;21(1):1–13.
22. Kachanov M, Tsukrov I, Shafiro B. Effective moduli of solids with cavities of various shapes. *Appl Mech Rev.* 1994;47(1S):S151–S174.
23. Sayers CM, Kachanov M. A simple technique for finding effective elastic constants of cracked solids for arbitrary crack orientation statistics. *Int J Solids Struct.* 1991;27(6):671–680.
24. Fortin J, Stanchits S, Vinciguerra S, Guéguen Y. Influence of thermal and mechanical cracks on permeability and elastic wave velocities in a basalt from Mt. Etna volcano subjected to elevated pressure. *Tectonophysics.* 2011;503(1-2):60–74.
25. Oda M, Takemura T, Aoki T. Damage growth and permeability change in triaxial compression tests of Inada granite. *Mech Mater.* 2002;34(6):313–331.
26. Schulze O, Popp T, Kern H. Development of damage and permeability in deforming rock salt. *Eng Geol.* 2001;61(2-3):163–180.
27. Vinciguerra S, Trovato C, Meredith PG, Benson PM. Relating seismic velocities, thermal cracking and permeability in Mt. Etna and Iceland basalts. *Int J Rock Mech Min Sci.* 2005;42(7-8):900–910.
28. Brace W, Walsh JB, Frangos WT. Permeability of granite under high pressure. *J Geophys Res.* 1968;73(6):2225–2236.
29. Benson P, Schubnel A, Vinciguerra S, Trovato C, Meredith P, Young RP. Modeling the permeability evolution of microcracked rocks from elastic wave velocity inversion at elevated isostatic pressure. *J Geophys Res: Solid Earth.* 2006;111(B4).
30. Faoro I, Vinciguerra S, Marone C, Elsworth D, Schubnel A. Linking permeability to crack density evolution in thermally stressed rocks under cyclic loading. *Geophys Res Lett.* 2013;40(11):2590–2595.
31. Gottesman T, Hashin Z, Brull M. Effective elastic moduli of cracked fiber composites. *Adv Compos Mater.* 1980;1:749–758.